

引用格式: XU Kuiwen, HOU Shasha, DENG Haoqian, et al. Limited-aperture Quantitative Inverse Imaging Based on Rytov Integral Approximation (Invited)[J]. Acta Photonica Sinica, 2023, 52(10):1052412

徐魁文,侯莎莎,邓皓千,等. 基于 Rytov 积分近似的有限口径定量反演成像(特邀)[J]. 光子学报, 2023, 52(10):1052412

基于 Rytov 积分近似的有限口径定量反演成像 (特邀)

徐魁文,侯莎莎,邓皓千,苏江涛,李文钧

(杭州电子科技大学 电子信息学院 射频电路与系统教育部重点实验室,杭州 310018)

摘要:提出一种适用于有限口径下高相对介电常数和大尺寸目标物体的反演方法。首先分析了低损耗介质的复折射率,通过有效折射率的计算方法得到有效折射率与介电常数关系;利用高频近似估计对比度函数,通过近似估计散射体内部散射场及其梯度对传统 Rytov 近似进行数学上的修正,产生无相位条件下 Rytov 积分近似模型,该模型可以实现定量重建高相对介电常数和大尺寸未知目标的对比度虚部。仿真结果显示有限口径下的 Rytov 积分近似可以对高介电常数和大尺寸目标的对比度虚部提供精确的形状重建。

关键词:计算电磁学;逆散射问题;电磁成像;有限口径;Rytov 积分近似;高相对介电常数

中图分类号:O441

文献标识码:A

doi:10.3788/gzxb20235210.1052412

0 引言

电磁逆散射问题是利用已知的人射场照射目标,通过入射电磁波与未知目标物体之间的相互作用,产生感应电流,二次散射的数据被外围的接收天线所接受,通过测量得到的散射场数据对未知目标区域中散射体的几何形状和物理参数(介电常数、电导率、磁导率等)进行重建。电磁逆散射由于可以对目标进行定量的反演成像,广泛应用于石油勘探、卫星遥感、生物医学成像等领域^[1-3]。由于接收的天线传感器数量远远小于被离散的未知数个数,所以电磁逆散射问题呈现出固有的病态性;同时电磁波在物体内部的多次逆散射效应导致严重的非线性,这些给问题求解带来了极大的挑战。

求解非线性逆散射问题主要有两种方法,一种是将非线性问题线性化,如玻恩近似反演方法(Born Approximation inversion method, BA)^[4]、直接采样法(Direct Sampling Method, DSM)^[5]、线性抽样法(Linear Sampling Method, LSM)^[6]等。这些方法适用于弱散射体,对于强散射体得到的结果较差。另一种方法是直接求解非线性方程,常用非迭代方法有后向传播算法(Back-Propagation, BP^[7])、扩展波恩近似方法(Extended Born Approximation, EBA^[8])。非迭代方法与线性方法类似仅适用于弱散射问题。非线性的迭代方法是将逆散射问题转化为最优化问题进行求解,主要包括对比源反演算法(Contrast Source Inversion, CSI)^[9]、子空间优化算(Subspace-based Optimization Method, SOM)^[10]、基于 SOM 方法提出的双重子空间法(Two-fold SOM, TSOM)^[11]和基于乘性正则化^[12]和快速傅里叶的 TSOM(a Fast Fourier Transform TSOM, FFT-TSOM)^[13]。相比于线性算法,非线性算法的反演能力强很多,但当未知目标介电常数和电尺寸增大时,迭代时间较长且容易陷入最优解导致反演失败。

上述提到的各种算法,无论是线性的还是非线性的都是指发射天线和接收天线均匀围绕在感兴趣区域周围的全口径成像方法。而在实际应用中,比如石油勘探、墙体检测,很难实现天线均匀围绕被测物体。为了拓展电磁反演成像的应用,提出了有限口径成像方法;即天线只分布在感兴趣区域的某边或某些角度。

基金项目:国家自然科学基金(Nos. 62293493, 61971174)

第一作者(通讯作者):徐魁文, kuiwenxu@hdu.edu.cn

收稿日期:2023-06-30;录用日期:2023-08-31

<http://www.photon.ac.cn>

但是有限口径会进一步增加电磁逆散射问题的非线性,目前基于有限口径的电磁反演成像研究很少,多数是关于电子计算机断层扫描(Computed Tomography, CT)成像^[14-15]的研究。因此本文提出一种基于Rytov积分近似的方法用于实现有限口径下高相对介电常数和大尺寸目标物体的定量反演成像。

1 逆散射模型

基于有限口径的二维电磁逆散射模型如图1所示,图中的矩形称为感兴趣区域(Domain Of Interest, DOI),目标物体存在于DOI内,发射天线和接收天线均匀分布在DOI两侧,图中天线代表发射天线或者接收天线。

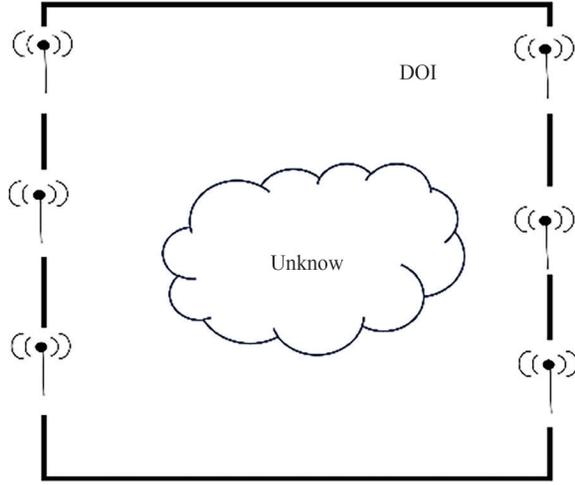


图1 有限口径下电磁逆散射成像模型

Fig. 1 Electromagnetic inverse scattering model under limited aperture

1.1 无相位Rytov近似

当DOI内没有散射体时,设 $E_i(\mathbf{r})$ 为DOI内某点 \mathbf{r} 处的入射场,满足自由空间亥姆霍兹方程,即

$$(\nabla^2 + k_0^2)E_i(\mathbf{r}) = 0 \quad (1)$$

式中, $k_0 = 2\pi/\lambda$ 为自由空间波数。当DOI内放入散射体时,总场定义为 $E_t(\mathbf{r})$,满足非均匀亥姆霍兹方程,其中 $n(\mathbf{r})$ 为折射率,即

$$(\nabla^2 + k_0^2 n^2(\mathbf{r}))E_t(\mathbf{r}) = 0 \quad (2)$$

引入散射场的复相位函数 $\varphi_s(\mathbf{r})$,表示与入射场的相位和对数振幅偏差,可将Rytov积分近似^[16]表示为

$$\frac{E_t(\mathbf{r})}{E_i(\mathbf{r})} = \exp(jk_0\varphi_s(\mathbf{r})) \quad (3)$$

由式(1)~(3)求得非线性微分方程

$$\nabla^2 E(\mathbf{r}) + k_0^2 E(\mathbf{r}) = -k_0^2 [(n(\mathbf{r})^2 - 1) - \nabla\varphi_s(\mathbf{r}) \cdot \nabla\varphi_s(\mathbf{r})] E_i(\mathbf{r}) \quad (4)$$

式中, $E(\mathbf{r}) = E_t(\mathbf{r}) \ln(E_t(\mathbf{r})/E_i(\mathbf{r}))$ 。

将式(4)转化为积分形式,得

$$\frac{E_t(\mathbf{r})}{E_i(\mathbf{r})} = \exp\left(\frac{k^2}{E_i(\mathbf{r})} \int g(\mathbf{r}, \mathbf{r}') [n(\mathbf{r}')^2 - 1 - \nabla\varphi_s(\mathbf{r}') \cdot \nabla\varphi_s(\mathbf{r}')] E_i(\mathbf{r}') dr'^2\right) \quad (5)$$

式中, $g(\mathbf{r}, \mathbf{r}')$ 表示背景介质的格林函数。

将式(5)乘以其共轭并两边取 \log_{10} 求得其无相位形式为

$$P_t(\mathbf{r}) = P_i(\mathbf{r}) + A \operatorname{Re} \left(\frac{k^2}{E_i(\mathbf{r})} \int g(\mathbf{r}, \mathbf{r}') \chi(\mathbf{r}') E_i(\mathbf{r}') dr'^2 \right) \quad (6)$$

式中, $A = 20 \log_{10} e$

$$\chi(\mathbf{r}') = n(\mathbf{r}')^2 - 1 - \nabla\varphi_s(\mathbf{r}') \cdot \nabla\varphi_s(\mathbf{r}') \quad (7)$$

在传统的Rytov积分近似中,由于式(6)的高度非线性通常省略 $\nabla\varphi_s \cdot \nabla\varphi_s$,当散射体为弱散射体时, $\nabla\varphi_s \cdot \nabla\varphi_s$ 的值很小,此时省略 $\nabla\varphi_s \cdot \nabla\varphi_s$ 的传统Rytov近似是有效的。当散射体为高介电常数的强散射体时, $\nabla\varphi_s \cdot \nabla\varphi_s$ 在反演过程中不能忽略,并且求解非线性方程式(5)极其困难,所以在低损介质中使用高频近似来获得 $\nabla\varphi_s \cdot \nabla\varphi_s$ 的近似^[17]。

1.2 低损耗介质

在低损耗介质中DOI中某点 r 处的折射率 $n(\mathbf{r})$ 和相对介电常数 $\epsilon_r(\mathbf{r})$ 变为复数,即^[18]

$$n(\mathbf{r}) = n_R(\mathbf{r}) + jn_I(\mathbf{r}) \quad (8)$$

$$\epsilon_r(\mathbf{r}) = \epsilon_R(\mathbf{r}) + j\epsilon_I(\mathbf{r}) \quad (9)$$

在低损耗介质中 $\epsilon_I \ll \epsilon_R$,根据折射率与相对介电常数之间的关系 $n^2(\mathbf{r}) = \epsilon_r(\mathbf{r})$ ^[19]可求得折射率实部和虚部与介电常数实部和虚部之间的关系为

$$n_R(\mathbf{r}) = \sqrt{\epsilon_R(\mathbf{r}) + \frac{1}{4}\delta^2(\mathbf{r})\epsilon_R(\mathbf{r})} \quad (10)$$

$$n_I(\mathbf{r}) = \frac{\epsilon_I(\mathbf{r})}{2\sqrt{\epsilon_R(\mathbf{r})}} = \frac{1}{2}\delta\sqrt{\epsilon_R(\mathbf{r})} \quad (11)$$

式中, $\delta(\mathbf{r})$ 表示介质的损耗正切角,通常定义为 $\delta(\mathbf{r}) = \epsilon_I(\mathbf{r})/\epsilon_R(\mathbf{r})$ 。

2 高频低损耗介质的近似

2.1 有效折射率

如图2所示为自由空间入射到有损介质,入射场在界面处被部分反射和透射,折射到散射体中的局部电磁波是不均匀的,此时折射率为复数,由Snell定理给出

$$\sin\theta_t = \sin\theta_i/n(\mathbf{r}) \quad (12)$$

式中, θ_t 和 θ_i 分别为折射角和入射角,如果折射率 $n(\mathbf{r})$ 的虚部不为0,此时折射角 θ_t 是一个复数,不能通过传统几何光学解释。通过引入有效折射率的概念^[20],入射场、反射场、透射场的电场矢量分量为

$$E_i(\mathbf{r}) = E_0 \exp(jk_0 \mathbf{e}_i \cdot \mathbf{r}) \quad (13)$$

$$E_r(\mathbf{r}) = E_1 \exp(jk_0 \mathbf{e}_r \cdot \mathbf{r}) \quad (14)$$

$$E_t(\mathbf{r}) = E_2 \exp(jk_0 (N_R \mathbf{e}_t \cdot \mathbf{r} + jN_I n_1 \cdot \mathbf{r})) \quad (15)$$

式中, N_R 和 N_I 分别为有效折射率的实部和虚部; \mathbf{e}_i 、 \mathbf{e}_r 和 \mathbf{e}_t 分别表示入射、反射和透射方向的单位向量。

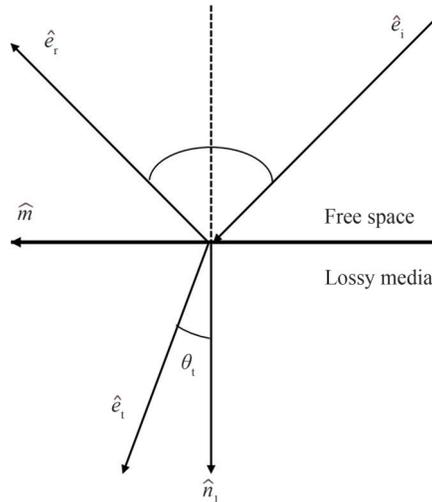


图2 自由空间入射到有损介质
Fig. 2 Free space incident on lossy media

入射场、反射场和透射场的相位应在介质界面切向匹配^[17]。如图 2 所示, 设与界面相切的向量为 m , 可以得到

$$m \cdot e_i = m \cdot e_r = m \cdot (N_R e_t + jN_1 n_1) \quad (16)$$

$$\sin \theta_i = \sin \theta_r = N_R \sin \theta_t \quad (17)$$

将式(15)中的电场矢量空间分量带入到波动方程式(2), 并使用式(16)和(17)求得有效折射率与实际折射率的关系为

$$N_R^2 - N_1^2 = n_R^2 - n_1^2 \quad (18)$$

$$N_R N_1 \cos \theta_t = n_R n_1, \quad e_t \cdot n_1 = \cos \theta_t \quad (19)$$

求解得到有效折射率与实际折射率的关系为

$$N_R = \sqrt{\frac{1}{2} \left(\sqrt{(n_R^2 - n_1^2)^2 + 4 \left(\frac{n_R n_1}{\cos \theta_t} \right)^2} + n_R^2 - n_1^2 \right)} \quad (20)$$

$$N_1 = \frac{n_R n_1}{N_R \cos \theta_t} \quad (21)$$

当介质为低损耗时, 通过 1.2 节中折射率与介电常数的关系可以求得实际折射率与介电常数关系, 即

$$N_R \approx n_R \left(1 + \frac{\sin \theta_t}{2(n_R^2 - \sin^2 \theta_t)} \delta^2 \right) \approx n_R \approx \sqrt{\epsilon_R} \quad (22)$$

$$N_1 \approx \frac{n_R n_1}{\sqrt{n_R^2 - \sin^2 \theta_t}} \left(1 - \frac{n_R^2 \sin^2 \theta_t}{2(n_R^2 - \sin^2 \theta_t)} \delta^2 \right) \approx \frac{n_R n_1}{\sqrt{n_R^2 - \sin^2 \theta_t}} \approx \frac{\epsilon_1}{2\sqrt{\epsilon_R - \sin^2 \theta_t}} \quad (23)$$

2.2 $\nabla \varphi_s \cdot \nabla \varphi_s$ 近似

使用 2.1 节中得到的关系, 结合图 2 沿射线方向 ($dr = dr e_t$), 将透射场电场矢量方程表示为

$$E_t(\mathbf{r}) = E_2 \exp(jk_0 (N_R dr e_t \cdot e_t + jN_1 dr n_1 \cdot e_t)) = E_2 \exp(-k_0 N_1 dr \cos \theta_t) \exp(jk_0 N_R dr) \quad (24)$$

对于折射率分段均匀分布的有损散射体, 按照沿射线方向的路径写成积分形式, 即

$$E_t(\mathbf{r}) = E_2 \exp\left(-k_0 \int N_1 \cos \theta_t dr\right) \exp\left(jk_0 \int N_R dr\right) \quad (25)$$

根据式(3)和入射场的电场矢量方程可求得 φ_s 为

$$\varphi_s(\mathbf{r}) = \frac{1}{jk_0} \ln \left[\frac{E_2}{E_1} \exp\left(\left(-k_0 \int N_1 \cos \theta_t dr\right) \exp\left(jk_0 \int N_R dr\right)\right) \right] = \frac{1}{jk_0} \ln \frac{E_2}{E_0} + \left[\int N_R dr - e_i \cdot \mathbf{r} + j \int N_1 \cos \theta_t dr \right] \quad (26)$$

从而得到

$$\begin{aligned} \nabla \varphi_s(\mathbf{r}) \cdot \nabla \varphi_s(\mathbf{r}) &= N_R^2 + 1 - 2N_R (e_t \cdot e_i) - N_1^2 + 2j(N_R e_t - e_i) \cdot N_1 n_1 - \\ &\quad \frac{1}{k_0^2} \left(\nabla \ln \frac{E_2}{E_0} \cdot \nabla \ln \frac{E_2}{E_0} \right) - j \frac{2}{k_0} \left(\nabla \ln \frac{E_2}{E_0} \right) \cdot ((N_R e_t - e_i) + jN_1 n_1) \end{aligned} \quad (27)$$

由图 2 可以看出 $e_i \cdot n_1 = \cos \theta_i$, $e_t \cdot e_i = \cos \theta_s$, 其中 θ_s 定义为散射角, 可以把式(27)转化为

$$\begin{aligned} \nabla \varphi_s(\mathbf{r}) \cdot \nabla \varphi_s(\mathbf{r}) &= N_R^2 + 1 - 2N_R \cos \theta_s - N_1^2 - \frac{1}{k_0^2} \left(\nabla \ln \frac{E_2}{E_0} \cdot \nabla \ln \frac{E_2}{E_0} \right) + \frac{2}{k_0} \nabla \ln \frac{E_2}{E_0} \cdot N_1 n_1 + \\ &\quad 2j \left((N_R N_1 \cos \theta_t - N_1 \cos \theta_i) - \frac{1}{k_0} \nabla \ln \frac{E_2}{E_0} \cdot (N_R e_t - e_i) \right) \end{aligned} \quad (28)$$

2.3 对比度近似

由 2.2 节中得到 $\nabla \varphi_s(\mathbf{r}) \cdot \nabla \varphi_s(\mathbf{r})$ 的近似结果, 求得不省略 $\nabla \varphi_s(\mathbf{r}) \cdot \nabla \varphi_s(\mathbf{r})$ 的 Rytov 积分近似的对比度函

数为

$$\chi(\mathbf{r}) = 2N_R \cos \theta_s - 2 + \frac{1}{k_0^2} \left(\nabla \ln \frac{E_2}{E_0} \cdot \nabla \ln \frac{E_2}{E_0} \right) - \frac{2}{k_0} \nabla \ln \frac{E_2}{E_0} N_1 \mathbf{n}_1 + j \left(2N_1 \cos \theta_i + \frac{2}{k_0} \nabla \ln \frac{E_2}{E_0} (N_R \mathbf{e}_t - \mathbf{e}_i) \right) \quad (29)$$

在高频低损耗条件下,结合有效折射率、实际折射率、和介电常数三者之间的关系求得对比度函数为

$$\chi(\mathbf{r}) = 2 \left(\sqrt{\epsilon_R} \cos \theta_s - 1 \right) + \frac{1}{k_0^2} \left(\nabla \ln \frac{E_2}{E_0} \cdot \nabla \ln \frac{E_2}{E_0} \right) - \frac{2}{k_0} \nabla \ln \frac{E_2}{E_0} N_1 \mathbf{n}_1 + j \left(\frac{\epsilon_1}{\sqrt{\epsilon_R - \sin^2 \theta_i}} \cos \theta_i + \frac{2}{k_0} \nabla \ln \frac{E_2}{E_0} (n_R \mathbf{e}_t - \mathbf{e}_i) \right) \quad (30)$$

当频率较高时(大于1 GHz),式(30)中的交叉项中包含 $1/k_0$ 和 $1/k_0^2$,只要 $\nabla \ln \frac{E_2}{E_0}$ 项的值很小,省略交叉项的近似就是有效的。在成像中假设物体在很大程度上是均匀的,因此 $\nabla \ln \frac{E_2}{E_0}$ 在物体内外都是最小的,省略交叉项是可行的,即

$$\chi(\mathbf{r}) = 2 \left(\sqrt{\epsilon_R} \cos \theta_s - 1 \right) + j \frac{\epsilon_1}{\sqrt{\epsilon_R - \sin^2 \theta_i}} \cos \theta_i \quad (31)$$

由式(31)可以看出,对比度函数的虚部是入射角 θ_i 和介电常数实部和虚部的函数,对比度函数的实部是散射角 θ_s 和介电常数实,重建的虚部分量中的任何失真都与物体的介电常数无关^[17],所以在成像中仅使用虚部分量。为部的函数。入射角 θ_i 只是物体形状的函数不随介电常数的变化而变化,散射角 θ_s 取决于 θ_i 和物体的介电常数,由于 θ_i 的存在了使虚部分量易于成像,通过取各种照射方向的平均值来去除虚部分量对入射角的依赖性,可得成像中使用的对比度函数的最终形式为

$$\text{Im}(\chi) = \frac{1}{\pi} \int_{-\frac{\pi}{2}}^{\frac{\pi}{2}} \frac{\epsilon_1}{\sqrt{\epsilon_R - \sin^2 \theta_i}} \cos \theta_i d\theta_i = \frac{2\epsilon_1}{\pi} \arcsin \left(\frac{1}{\sqrt{\epsilon_R}} \right) \quad (32)$$

3 仿真示例

设置工作频率为2.4 GHz,感兴趣区域(DOI)选择为3 m×3 m的矩形区域,区域中心与原点重合。在DOI左右两侧的边界处分别放置20个天线,这些天线既可作为发射天线也可作为接收天线。计算前向问题时,都将感兴趣区域剖分为240×240个小网格,在逆问题中,将感兴趣区域剖分为120×120个小网格。在逆问题求解中使用增强拉格朗日和交替方向算法的TV最小化(TV AL3)的正则化方法^[21]。

3.1 示例1

工作频率设置为2.4 GHz,在感兴趣区域中心处放置半径为2λ的圆,如图3所示,X轴Y轴单位为m,分别选择4组不同介电常数值,弱散射体($\epsilon_R \approx 1, \epsilon_R \gg \epsilon_1$)(第一行, $\epsilon_R = 1.1, \epsilon_1 = 0.11, \text{Im}(\chi) = 0.0886$);中等散射体($\epsilon_R > 1, \epsilon_R \gg \epsilon_1$)(第二行, $\epsilon_R = 5, \epsilon_1 = 0.5, \text{Im}(\chi) = 0.1476$);强散射体($\epsilon_R \gg 1, \epsilon_R \gg \epsilon_1$)(第三行, $\epsilon_R = 15, \epsilon_1 = 1.5, \text{Im}(\chi) = 0.2494$);第四行, $\epsilon_R = 50, \epsilon_1 = 5, \text{Im}(\chi) = 0.4517$)。

如图3所示,当目标为弱散射体时,有限口径可以比较准确地重建出对比度的虚部。将介电常数提高到 $\epsilon_R = 5, \epsilon_1 = 0.5$,此时目标为中等散射体,虽然重建结果的幅值有小幅度衰减,但是可以提供精确的形状重建;当目标为强散射体时,重建结果的幅值衰减是可以预估的,在求对比度近似时当介电常数实部和虚部非常大时,近似引起的误差也被放大,这会影响重建的结果。图3结果表明,有限口径下的Rytov积分近似算法可以实现高介电常数和大尺寸物体形状的精准重建,但当介电常数太大时,重建结果的幅度会有衰减;这

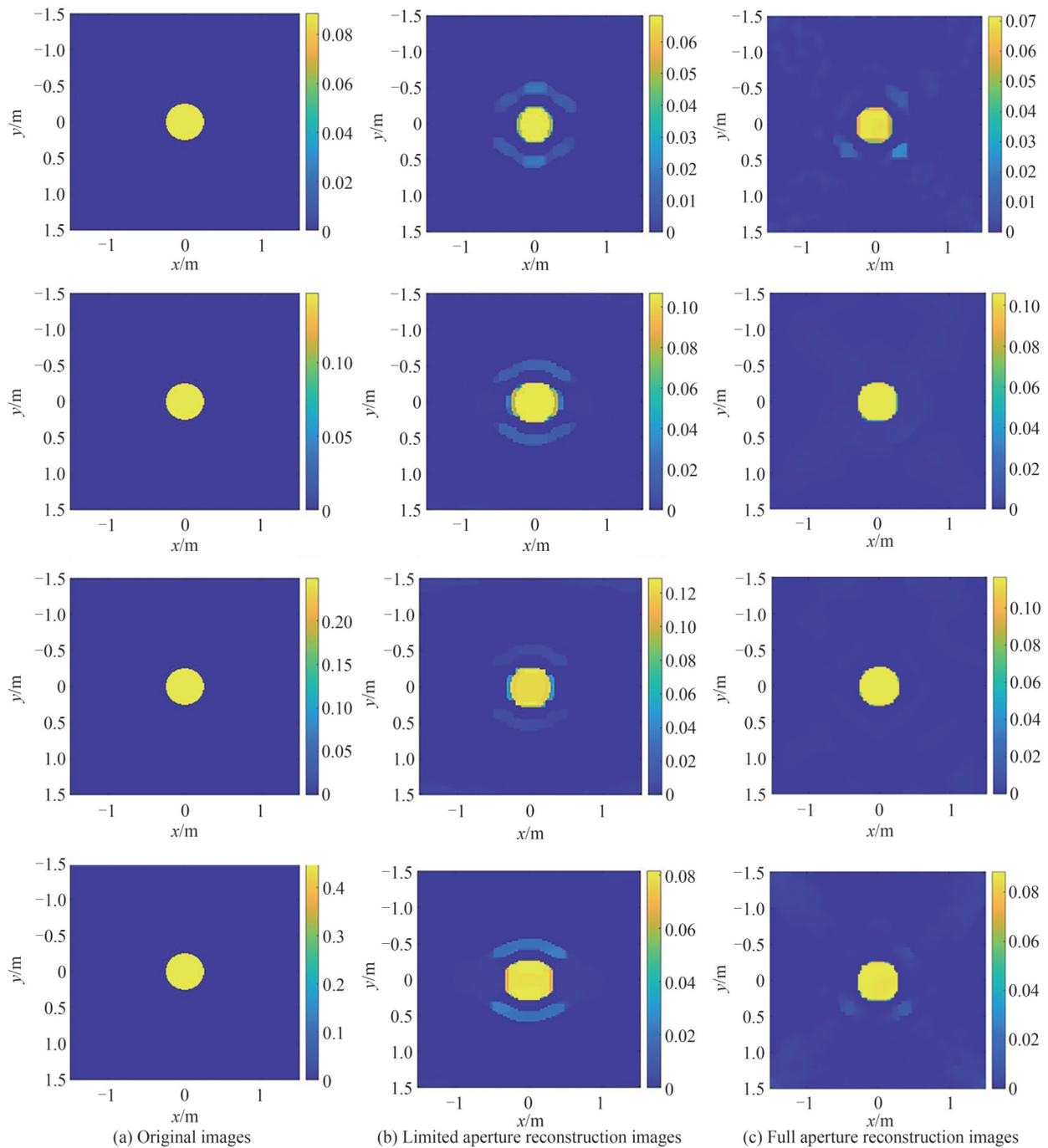


图3 有限口径与全口径成像对比

Fig. 3 Limited aperture versus full aperture reconstruction images

种幅值的衰减在全口径时也无法避免。

3.2 示例 2

在中等散射($\epsilon_R = 5, \epsilon_I = 0.5$)条件下,图4中第一行是与之前不同的散射体形状,边长为 5λ 的矩形;第二行散射体为半径为 5λ 的圆形。由仿真结果可以看出图4中矩形也有很好的重建结果。从图3和图4不同形

状和不同尺寸的重建结果可以看出,在中等散射条件下该算法也有很好的重建结果。

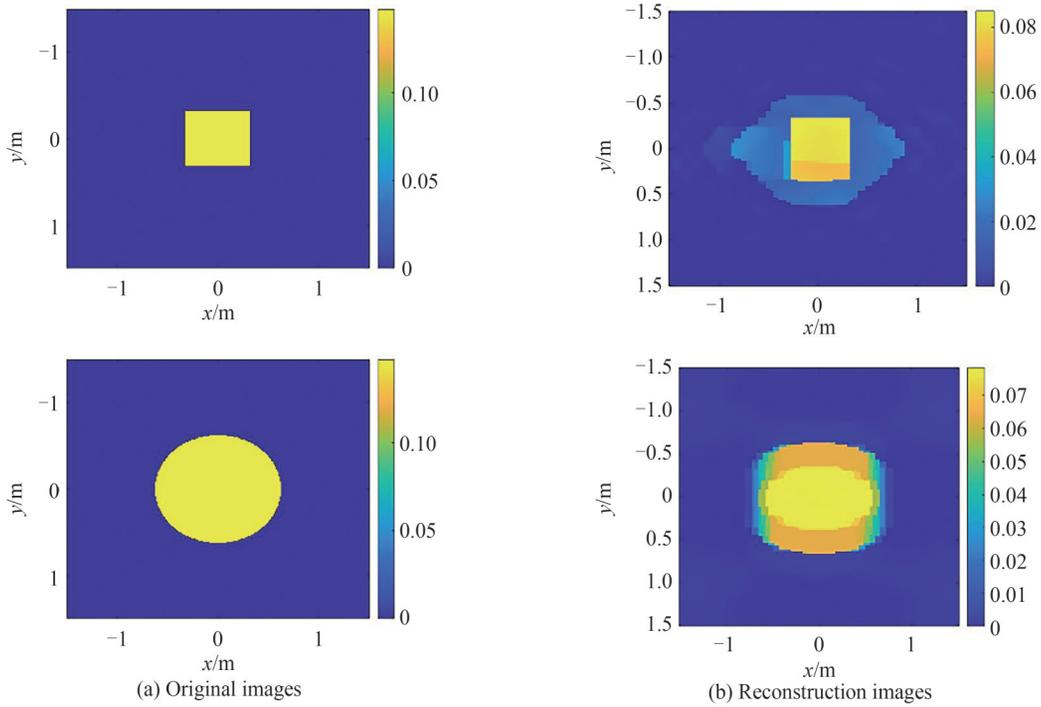


图4 中等散射体不同形状重建结果

Fig. 4 Reconstruction results for different shapes of medium scatterers

3.3 示例3

在示例1的基础上,再次反演中等散射($\epsilon_R = 5, \epsilon_I = 0.5$)和强散射目标($\epsilon_R = 15, \epsilon_I = 1.5$),向测量数据中加入高斯白噪声来验证算法的鲁棒性。图5可以清楚地看到,在加入10%噪声情况下,重建结果与图3相比几乎没有影响。

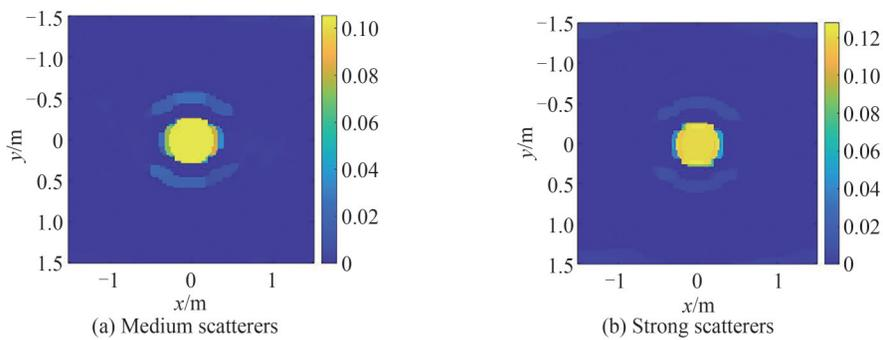


图5 加入高斯白噪声后的重建结果

Fig. 5 Reconstruction images after adding Gaussian white noise

3.4 示例4

在本实例中选择圆形目标,如图6所示,在示例1的基础上减少天线的数目,左右两边各摆放10个天线,反演中等散射($\epsilon_R = 5, \epsilon_I = 0.5$)和强散射目标($\epsilon_R = 15, \epsilon_I = 1.5$);当天线数目减少后仍然可以重建出目标的形状。如图7,减少天线数目为左右两边各摆放5个天线,反演中等散射($\epsilon_R = 5, \epsilon_I = 0.5$)和强散射($\epsilon_R = 15, \epsilon_I = 1.5$)目标,由重建结果可以看出当天线数目过少时无法分辨出目标形状。如图8,改变工作频率设

置,选择中等散射($\epsilon_r = 5, \epsilon_i = 0.5$)目标,频率为 1.5 GHz 和 3 GHz,由重建结果可以看出,增加工作频率和降低工作频率后仍然可以重建出目标形状。

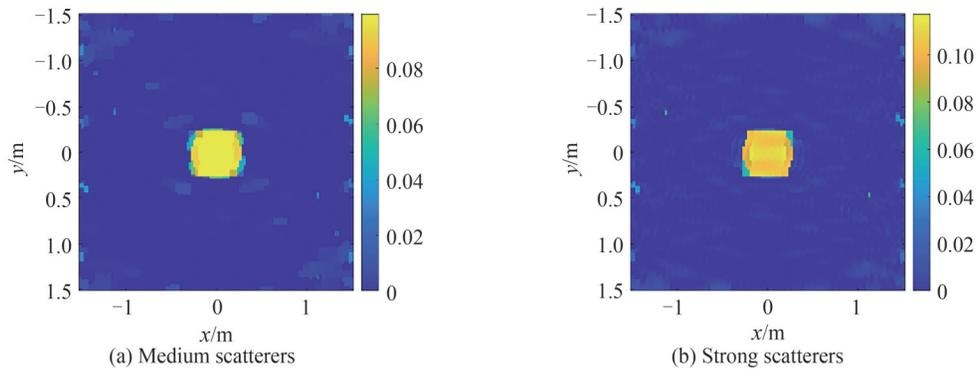


图6 减少天线数目为左右两边各10个的重建结果

Fig. 6 Reconstruction results after reducing the number of antennas to 10 on each left and right side

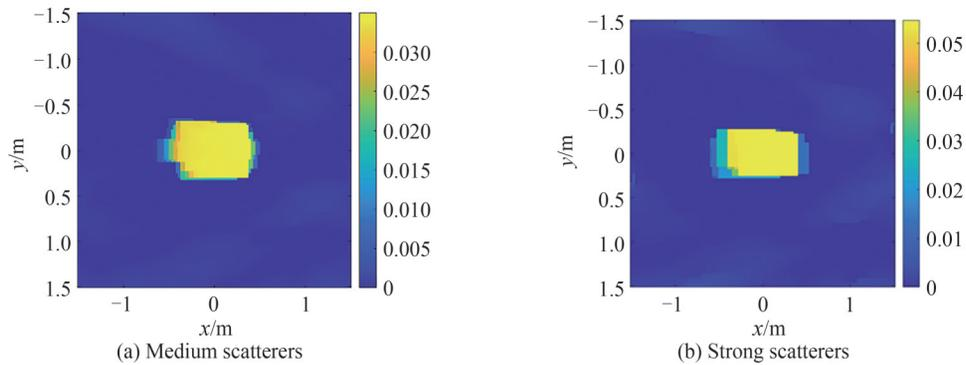


图7 减少天线数目为左右两边各5个的重建结果

Fig. 7 Reconstruction results after reducing the number of antennas to 5 on each left and right side

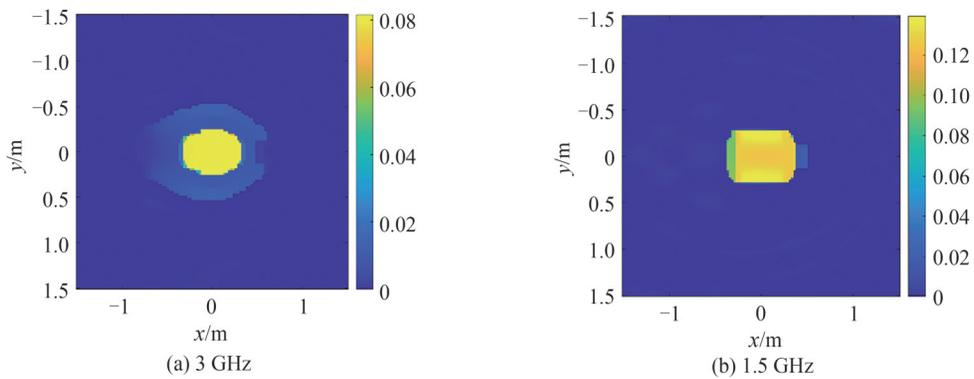


图8 改变频率后的重建结果

Fig. 8 Reconstruction results for changing frequency

3.5 示例5

在本示例选择正方形目标,图9为多目标物体重建结果。分别选择中等散射($\epsilon_r = 5, \epsilon_i = 0.5$)和强散射

目标 ($\epsilon_R = 15, \epsilon_I = 1.5$), 天线数目为左右两边各 20 个。当重建目标变复杂时, 该算法也能大致重建出目标形状。如图 10, 改变天线布局为 L 型摆放, 图 11 为弱散射条件下 L 型天线摆放重建结果, 改变天线布局后弱

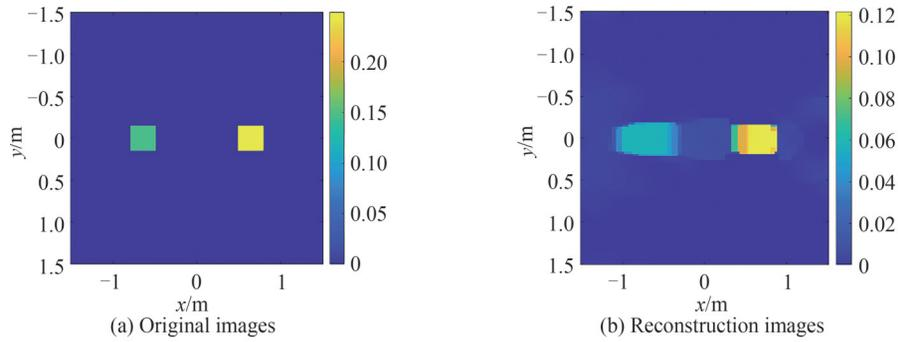


图 9 多目标物体重建结果
Fig. 9 Multiple target object reconstruction results

散射条件下可以较好地重建目标。

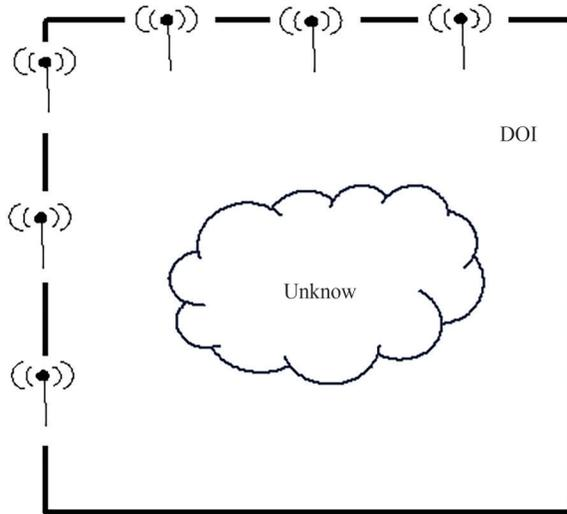


图 10 重构天线布局
Fig. 10 Modified antenna layout

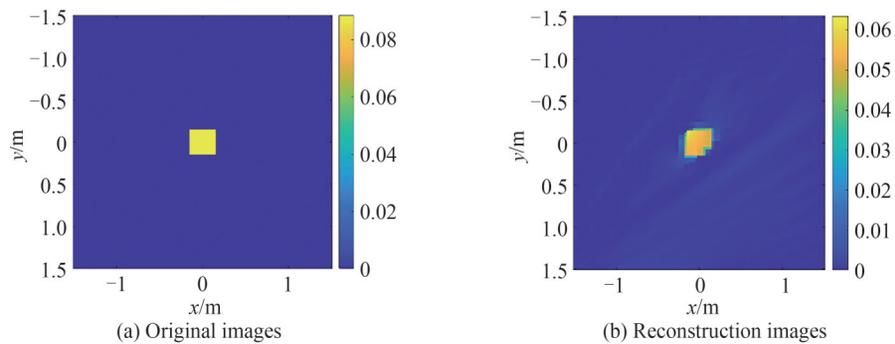


图 11 重构天线布局重建结果
Fig. 11 Reconstruction results for modified antenna layout

4 结论

本文基于 Rytov 积分近似, 提出了一种有限口径下高介电常数和大尺寸目标的电磁定量反演方法。通过近似估计散射体内部散射场, 以及利用梯度对传统 Rytov 近似进行数学上修正, 产生无相位条件下 Rytov

积分近似模型。仿真结果表明该算法在有限口径下对高介电常数和大尺寸目标的中等散射体目标提供了对比度函数虚部分量较好的定量重建结果;也可对强散射体的对比度函数虚部分量提供形状的精确重建。此外该方法还具有较好的抗噪声能力,有望在医疗成像、无损检测以及探地雷达中得到广泛的应用,在后续工作中拟针对三维目标的快速反演进行探索,为工程应用提供技术支撑。

参考文献

- [1] SONG X, LI M, YANG F, et al. Three-dimensional joint inversion of acoustic and electromagnetic data based on contrast source inversion[C]. 2019 IEEE International Symposium on Antennas and Propagation and USNC-URSI Radio Science Meeting, 2019: 1023-1024.
- [2] KONER P K, HARRIS A, MATURI E. A physical deterministic inverse method for operational satellite remote sensing: an application for sea surface temperature retrievals[J]. IEEE Transactions on Geoscience and Remote Sensing, 2015, 53(11): 5872-5888.
- [3] CHANDRA R, ZHOU H, BALASINGHAM I, et al. On the opportunities and challenges in microwave medical sensing and imaging[J]. IEEE Transactions on Biomedical Engineering, 2015, 62(7): 1667-1682.
- [4] KAZEMIVALA R, TAJIK D, NIKOLOVA N K. Simultaneous use of the born and rytov approximations in real-time imaging with Fourier-space scattered power mapping[J]. IEEE Transactions on Microwave Theory and Techniques, 2022, 70(5): 2904-2920.
- [5] CATAPANO I, CROCCO L, ISERNIA T. On simple methods for shape reconstruction of unknown scatterers[J]. IEEE Transactions on Antennas and Propagation, 2007, 55(5): 1431-1436.
- [6] DOGU S, AKINCI M N. Assessment of linear sampling method and factorization method for through the wall imaging[C]. 2018 26th Telecommunications Forum (TELFOR), 2018: 420-425.
- [7] WEI Zhun, CHEN Xudong. Deep-learning schemes for full-wave nonlinear inverse scattering problems [J]. IEEE Transactions on Geoscience and Remote Sensing, 2018, 57(4): 1849-1860.
- [8] CHEW W C, WANG Y M. Reconstruction of two-dimensional permittivity distribution using the distorted born iterative method[J]. IEEE Transactions on Medical Imaging, 1990, 9(2): 218-225.
- [9] RAN Peipei, QIN Yingying, LESSELIER D, et al. Subwavelength microstructure probing by binary-specialized methods: contrast source and convolutional neural networks[J]. IEEE Transactions on Antennas and Propagation, 2021, 69(2): 1030-1039.
- [10] CHEN Xudong. Subspace-based optimization method for solving inverse-scattering problems [J]. IEEE Transactions. Geoscience and Remote Sensing, 2010, 48(1):42-49.
- [11] ZHONG Yu, CHEN Xudong. Twofold subspace-based optimization method for solving inverse scattering problems[J]. Inverse Problems: An International Journal of Inverse Problems, Inverse Methods and Computerised Inversion of Data, 2009, 25(8): 1-11.
- [12] XU Kuiwen, ZHONG Yu, SONG Rencheng, et al. Multiplicative-regularized FFT twofold subspace-based optimization method for inverse scattering problems [J]. IEEE Transactions on Geoscience and Remote Sensing, 2015, 53(2): 841-850.
- [13] ZHONG Yu, CHEN Xudong. An fft twofold subspace-based optimization method for solving electromagnetic inverse scattering problems[J]. IEEE Transactions on Antennas and Propagation, 2011, 59(3): 914-927.
- [14] PIAUTI P, KING A, HENRY L, et al. A thresholding based iterative reconstruction method for limited-angle tomography data[J]. Tomography of Materials and Structures, 2023, 2(8): 100008.
- [15] ZHANG Z, YANG M, LI H, et al. An innovative low-dose ct inpainting algorithm based on limited-angle imaging inpainting model[J]. Journal of X-ray Science and Technology, 2022, 31(10): 1-22.
- [16] WU R S. Wave propagation, scattering and imaging using dual-domain one-way and one-return propagators[J]. Pure and Applied Geophysics, 2003, 160(3-4): 509-539.
- [17] DUBEY A, DESHMUKH S, PAN L, et al. A phaseless extended Rytov approximation for strongly scattering low-loss media and its application to indoor imaging[J]. IEEE Transactions on Geoscience and Remote Sensing, 2022, 60: 1-17.
- [18] ZHOU Li. Discussion of the refractive index problem[J]. Physics Teacher, 2014, 35(1): 60-61, 73.
周莉. 折射率问题的讨论[J]. 物理教师, 2014, 35(1): 60-61, 73.
- [19] HUANG Zhixun. Theory on the relative permittivity and refractive index of air[J]. Journal of Beijing Broadcasting Institute (Natural Science Edition), 1996, (3): 3-12.
黄志洵. 关于空气的相对介电常数与折射率的理论[J]. 北京广播学院学报(自然科学版), 1996, (3): 3-12.

- [20] PING Y, LIU K N. Effective refractive index for determining ray propagation in an absorbing dielectric particle [J]. *Journal of Quantitative Spectroscopy and Radiative Transfer*, 2008, 110(4):300-306.
- [21] LI Huibin. Effect of different measurement matrices on image reconstruction quality based on TVAL3 algorithm [J]. *Optoelectronics Applications*, 2018, 33(3):48-51.
- 李慧滨. 基于TVAL3算法不同测量矩阵对图像重构质量的影响[J]. *光电技术应用*, 2018, 33(3):48-51.

Limited-aperture Quantitative Inverse Imaging Based on Rytov Integral Approximation (Invited)

XU Kuiwen, HOU Shasha, DENG Haoqian, SU Jiangtao, LI Wenjun

(*Key Laboratory of Radio Frequency Circuits and Systems, Ministry of Education, School of Electronics and Information Engineering, Hangzhou Dianzi University, Hangzhou 310018, China*)

Abstract: Currently, there are two primary approaches to addressing nonlinear electromagnetic inverse scattering problems. One method involves linearizing these issues, while the other treats them as iterative optimization problems. However, a significant challenge arises in real-world applications, where achieving uniform antenna coverage around the target proves to be exceptionally difficult. To surmount this challenge, limited aperture imaging methods have been proposed. Although limited aperture imaging provides more significant flexibility, it amplifies the nonlinearity of electromagnetic inverse scattering problems, resulting in relatively limited research on this front.

This paper introduces a novel method founded on the limited aperture Rytov integral approximation for the purpose of quantitative inversion imaging of high relative permittivity and large-sized target objects. That is, the antennas are distributed only on one side of the region of interest or on some specific angles; limited aperture imaging provides greater flexibility. To begin, we introduce the concept of the phaseless Rytov approximation and meticulously analyze the complex refractive index within low-loss media. By analyzing the reflection and transmission of the incident field from the free space to the lossy media, the concept of effective refractive index is introduced and combined with Snell's theorem to solve the relationship between the effective refractive index and the actual refractive index, and the relationship between the actual refractive index and the dielectric constant is established according to the relationship between the dielectric constant and the refractive index in the low-loss media. Under the conditions of high frequency and low loss, we estimate the contrast function by taking into account the interplay between the effective refractive index, the actual refractive index, and the dielectric constant. We then employ mathematical corrections to approximate the scattered field and its gradient within the scattering object, thereby enhancing the traditional Rytov approximation. This enhancement results in the development of a phaseless limited aperture Rytov integral approximation model.

In the simulation section, three different scattering objects with varying strengths are selected, namely weak scatterers, medium scatterers, and strong scatterers. This model is capable of providing quantitatively better reconstruction results for weak and medium scatterers with different shapes, characterized by high permittivity and large target size. For strong scatterers, it accurately reconstructs the target shape by considering the imaginary component of the contrast function. Additionally, for multi-target scenarios, both medium and strong scatterers are well-reconstructed in terms of object shapes. Furthermore, the model also yields favorable results when altering the operating frequency and antenna placement layout. Lastly, this model exhibits strong noise resistance capabilities.

The proposed method is expected to be widely used in medical imaging, non-destructive testing and ground penetrating radar.

Key words: Computational electromagnetics; Inverse scattering problems; Electromagnetic imaging; Limited aperture; Rytov integral approximation; High relative dielectric constant

OCIS Codes: 290.3200; 290.5825; 110.1220